International Journal of Plasticity 50 (2013) 1–17

Contents lists available at SciVerse ScienceDirect

International Journal of Plasticity

journal homepage: www.elsevier.com/locate/ijplas

Strain rate effects on the mechanical response in multi- and single-crystalline Cu micropillars: Grain boundary effects

J.Y. Zhang, G. Liu *, J. Sun *

State Key Laboratory for Mechanical Behavior of Materials, Xi'an Jiaotong University, Xi'an 710049, PR China

ARTICLE INFO

Article history:
Received 20 November 2012
Received in final revised form 11 March 2013
Available online 29 March 2013

Keywords:
Cu pillar
Strain burst
Strength
Strain rate sensitivity
Grain boundary

ABSTRACT

Homogeneous interfaces like grain boundaries (GBs) play an important role in crystalline plasticity as they often serve as obstacles for dislocation motion, as well as dislocation sources/sinks. In the present work, microcompression experiments were carefully performed to uncover the effects of GBs on mechanical response of submicron-sized Cu multi-crystalline (MC) micropillars (containing several grains) by comparing with the single-crystalline (SC) samples at different strain rates. It is clearly demonstrated that, while the SC pillars suffer from intermittent and stochastic strain bursts, introducing GBs appropriately into the SC pillars can dramatically improve the smoothness of their plastic flow and enhance their strength and strain rate sensitivity (SRS), especially at greater strain rates. The presence of GBs can significantly suppress the strain bursts observed in the MC/SC Cu micropillars, which is simply quantified by considering the size and strain rate related-capacity of dislocation absorption by the GBs. These findings provide deep insights into the controllability of plastic deformation of small volume materials. The possible transition of strengthening mechanisms with plastic strain is also highlighted.

1. Introduction

Efforts to characterize the small-scaled and scale-specific mechanical properties of materials are driven by the need to provide design guidelines for reliable nano- and micro-electromechanical devices and a desire to develop detailed and accurate hierarchical models of the mechanical behavior of multicomponent structural materials (Hemker and Sharpe, 2007). A major current focus in the nanomechanical community is the investigation of single-crystalline (SC) strength at reduced dimensions through uniaxial deformation of micron- or nanopillars (Uchic et al., 2004; Greer et al., 2005). This is a fact that is classically neither expected nor comprehensively understood, but shown by numerous studies (for the reviews on this topic, see Refs. (Dehm, 2009; Uchic et al., 2009; Kraft et al., 2010; Greer and De Hosson, 2011)). The plastic deformation of these small volume SC pillars with non-zero initial dislocation densities beyond the elastic regime shows three unusual characteristics that are not observed in conventional bulk metals, *i.e.*, (i) Size-driven strength (σ), which can be empirically described by a power law: $\sigma = A\phi^{-n}$, where A is a constant, ϕ is sample diameter and n is power-law exponent, ranging from 0.5 to 1 (Dehm, 2009; Uchic et al., 2009; Kraft et al., 2010; Greer and De Hosson, 2011). Currently, the micro-mechanisms of size-dependent strengthening for such SC materials are commonly explained by dislocation starvation effect applicable at nano-scale (Greer and Nix, 2006; Shan et al., 2008; Huang et al., 2011; Zhou et al., 2011; Wang et al., 2012) and source truncation (Kiener et al., 2008; Oh et al., 2009; Kiener and Minor, 2011a) or source exhaustion (Rao et al., 2008; Akarapu et al., 2010; Kiener and Minor, 2011b) effects applicable at submicron- and micron-scale; (ii) Inherent intermittent and stochastic strain bursts (Dimiduk et al., 2006; Csikor et al., 2007; Friedman et al., 2012), which are caused by dislocation avalanches at large

* Corresponding authors. Tel.: +86 (0)2982668695; fax: +86 (0)2982663453.
E-mail addresses: lgsammer@mail.xjtu.edu.cn (G. Liu), junsun@mail.xjtu.edu.cn (J. Sun).

0749-6419/$ - see front matter © 2013 Elsevier Ltd. All rights reserved.
http://dx.doi.org/10.1016/j.ijplas.2013.03.009

size and mechanical annealing at small size (Greer and Nix, 2006; Shan et al., 2008; Huang et al., 2011; Zhou et al., 2011; Wang et al., 2012); and (iii) High strain rate sensitivity (SRS, m) and low activation volume (V^*) (Zhu et al., 2008; Schneider et al., 2009a; Jennings et al., 2011). Although such small-scaled materials are being considered for applications that take advantage of the high strength, their rate-limiting processes (m and V^*) remain lack of deep understanding. Specifically, the jumpy and stochastic nature of small-scaled SC materials often leads to an abrupt shape change (structural collapse), dramatically undercutting the desirable formability of small components. As this unique behavior emerges, a crucial question naturally arises: How to improve the controllability of plastic deformation of such small-scaled SC materials and to enable them to deform in a controlled manner within the maximum achievable plastic strain.

Most recent findings (Ng and Ngan, 2009; El-Awady et al., 2011; Jennings et al., 2012) have demonstrated that, because the strong barrier can significantly inhibits dislocations to vanish at the free surface (Zhou et al., 2012), the passivated SC pillars exhibit much greater strength and hardening relative to the unpassivated ones at an equivalent diameter. This is akin to that of polycrystalline Cu thin films with and without passivation (Gruber et al., 2008). Furthermore, unlike the uncoated SC pillar whose stress–strain response is jerky, the plastic flow of the coated SC pillar is much smoother (Ng and Ngan, 2009; El-Awady et al., 2011). Another viable route that can smoothen the plastic flow of SC materials is by increasing the density of preexisting defects, such as dislocations (Bei et al., 2008; El-Awady et al., 2013; Schneider et al., 2013) and solute atom clusters (Xie et al., 2013). These aforementioned results indicate that the deformation of SC pillars can become more controllable when dislocations are trapped inside them. Therefore, intentionally preventing mobile dislocations from annihilation such as introducing (several) grain boundaries (GBs) into small-scaled SC pillars to hinder dislocation motion should induce a fundamentally different mechanical performance. Through 3D-DDD simulations, (Csikor et al., 2007) further pointed out that the strain bursts caused by internal dislocation avalanches can be limited by the existence of GBs, which in turn renders appreciable smoothness of plastic flow in multi-crystalline (MC) materials containing several grains. However, the roles of internal GBs played in burst behavior are still unclear and the effects of homogeneous GBs on plastic characteristics such as strength, SRS and activation volume of these small-volume MC pillars are worthy of studying to understand the deformation mechanisms of small-scaled pillars.

Different from the small-scaled SC materials, there are abundant GBs in conventional polycrystalline metals. The GBs in bulk polycrystalline metals provide effective barriers to transmission of dislocations from one grain to the next, which leads to strengthening via a well-known Hall–Petch mechanism (Arzt, 1998; Pande and Cooper, 2009). When the grain size (d) falls below a critical value (at nanoscale $\sim$15 nm), the role of GBs shifts toward dislocation nucleation/absorption sites and sometimes to the deformation path itself (Meyers et al., 2006; Zhu and Li, 2010), which leads to the so-called "inverse Hall–Petch relation" in nanocrystaline (NC) materials (Schiotz and Jacobsen, 2003; Barai and Weng, 2009). Due to more dislocation-GB interactions, the bulk fcc nanostructures, such as Ni (Schwaiger et al., 2003; Wang et al., 2006) and Cu (Lu et al., 2005; Chen et al., 2006) also exhibit higher SRS (and smaller V^*) than their bulk counterparts (Dao et al., 2007). The increased SRS with reduction in characteristic size observed in polycrystalline fcc materials has been quantified by varies theoretical modes (Cheng et al., 2005; Li and Weng, 2007; Gu et al., 2011) at different length-scales. To date, it is well established that for fcc metals, deformation via the motion of dislocations produced from the bulk sources (Frank–Read sources or single-arm sources) usually induces lower SRS (and greater $V^* \sim 100b^3 - 1000b^3$), while deformation via dislocation nucleation from the boundaries usually induces higher SRS (and smaller $V^* \sim 1b^3 - 10b^3$) (Zhu et al., 2008; Lu et al., 2009c; Zhu and Li, 2010; Jennings et al., 2011). Therefore, this great difference in V^* should manifest itself in vastly different $\dot{\varepsilon}$ dependences between these two mechanisms, with GBs/surface sources being more sensitive to $\dot{\varepsilon}$ than bulk sources.

Although tremendous efforts have been dedicated to investigating the robust mechanical performance of small-scaled SC pillars and bulk polycrystalline materials, the mechanical response of the small-sized MC pillars remains unexplored. Yet the effects of internal microstructure dimension and external size limitation on plastic flow are likely to interplay with each other and need to be deeply understood. Also, it is natural to ask to what degree the GBs influence the SRS of MC materials at micro- and nano-scale. In this work, we systematically investigate the SRS of MC Cu pillars with diameter (ϕ = 500–1200 nm) to grain size ($d \approx 180$ nm) ratios ($\eta = \phi/d$) $\sim$ 3–7 and that of SC Cu pillars with diameters (ϕ) spanning from 600 to 1200 nm at different strain rates to fully understand the influence of GBs on deformation of MC/SC pillars. We demonstrate that if dislocations are trapped inside a small crystal, then the problem of intermittent and stochastic strain burst behavior can be alleviated, and more stable strain hardening can be achieved. The size- and strain rate-related burst behaviors are quantitatively explained by considering the dislocations nucleated from boundaries/bulk sources and statistically absorbed by boundaries.

2. Experimental procedures

2.1. Cu films synthesis and microstructure characterization

At room temperature, two types of Cu films were prepared on Si substrate by direct current magnetron sputtering at different deposition rates. One is the $\sim$1.6 μm-thick Cu films with submicron sized grains and the other is $\sim$2 μm-thick Cu films with several microns sized grains. The chamber was evacuated to a base pressure of $\sim 6.0 \times 10^{-8}$ torr prior to sputtering, and $\sim 2.0 \times 10^{-3}$ torr Ar were used during deposition. The X-ray diffraction (XRD) experiment was carried out using an improved Rigaku D/max-RB X-ray diffractometer with Cu Kα radiation and a graphite monochromator to determine the crystallographic

texture. Transmission electron microscopy (TEM) observation was performed using a JEOL-2100 high-resolution electron microscopy (HRTEM) with 200 kV accelerating voltages to observe the microstructure features of Cu films.

2.2. Fabrication of Cu micropillars

The MC Cu micropillars with ϕ = 500–1200 nm and SC Cu micropillars with ϕ = 600–1200 nm were respectively fabricated from the ~1.6 and ~2 μm-thick Cu films using the focused ion beam (FIB) technique in a Helios 600 Dual Beam instrument, which also allows scanning electron microscopy (SEM) imaging. The Cu pillars preparation process consisted of two steps, following the approach adopted by Greer et al. (2005). The current as low as 20 pA was used to minimize any damage due to Ga ion beam and to clean any redeposited materials from the pillar surface. A protective coating layer was not employed in the present work to avoid any contribution to the mechanical response from the presence of foreign layers. The dimensions of the Cu pillars and the taper were measured from SEM images. The aspect (height-to-diameter) ratios of the pillars varied between 1.3 and 3.2 for the MC pillars while it varied between 1.7 and 3.5 for the SC pillars. The small aspect ratios can avoid the bucking of pillars (Kiener et al., 2009a). The taper angles (ψ) of the pillars were measured between 2° and 4°.

2.3. Flat punch compression test

The microcompression test was performed on a Hystron Ti 950 with a 10 μm side-flat quadrilateral cross-section diamond indenter. The alignment of tip-pillar was achieved with the help of an optical microscope. All of the micropillars were compressed under the displacement-controlled mode at strain rates ($\dot{\varepsilon}$) spanning from 2×10^{-4} to 2×10^{-2} s^{-1} up to ~30% strain, which was followed by a holding segment of 5 s prior to unloading. Following our previous works (Zhang et al., 2012c,b), an attempt was made to correct for the compliance of the base of the pillar by using the model of a perfectly rigid circular flat punch being indented onto an isotropic half space first proposed by Sneddon (1965). To improve the reliability and accuracy of the present measurements, great efforts were devoted to the correction of thermal drift in the microcompression test. In the present work, the allowable-drift-rate was set at 0.005 nm s^{-1}, which is 20 times smaller than the typical value (0.1 nm s^{-1}) generally used in typical nanoindentation/micropillars compression tests. If the drift rate exceeded 0.01 nm s^{-1}, the experimental data was discarded. Therefore, in present mechanical test, the effect of thermal drift could be minimized and neglected. Force-displacement data were continuously recorded, and the initial geometry of the pillar was measured from the SEM images. The cross-sectional area at half height of the pillar (A_0) and the initial height (L_0) were used for calculations. True stress–strain curves were employed to characterize the deformation behavior (Greer et al., 2005; Bharathula et al., 2010). More details about the calculation procedure of the true stress–strain curves can be referred to Refs. (Greer et al., 2005; Bharathula et al., 2010). After the considerations of substrate effect and taper correction, the true strain ε_T and true stress σ_T are simply expressed as:

$$\varepsilon_T = \frac{1}{E_{Cu}}\frac{PL_p}{A_0L_0} + \ln\left(\frac{L_0}{L_p}\right) = \frac{1+\frac{L_0}{r_0}\tan\psi}{E_{measured}}\frac{PL_p}{A_0L_0} + \ln\left(\frac{L_0}{L_p}\right), \tag{1}$$

and

$$\sigma_T = \frac{P}{A_p} = \frac{PL_p}{A_0L_0} = \frac{P}{A_0L_0}\left\{L_0 - \left[u_{tot} - \frac{\sqrt{\pi}P(1-\nu_{Cu}^2)}{2E_{Si}\sqrt{A_{Si}}}\right]\right\}, \tag{2}$$

where A_0 is the cross-sectional area at half initial height (L_0) of the pillar; r_0 is the radius at the top of the pillar; L_p and A_p are the final height and average cross-sectional area, respectively; P is the load; E_{Cu} is the true modulus of Cu pillars without tapers and $E_{measured}$ is the measured modulus of the tapered Cu pillars; u_{tot} is the total displacement; ν_{Cu} is the Poisson's ratio of the Cu (~0.343); A_{Si} and E_{Si} is respectively the average cross-sectional area and the modulus of the substrate Si pillar. Note the influence of taper (ψ) has been taken into account in above equations.

3. Experimental results

3.1. Microstructure of MC/SC Cu pillars

XRD results revealed that the ~1.6 μm-thick Cu films exhibited a polycrystalline structure with random orientations, while the ~2 μm-thick Cu films showed a quasi-SC structure with strong (100) texture, within which the ⟨100⟩SC Cu pillars were fabricated by FIB. Cross-sectional and planar TEM observations of the polycrystalline Cu films show the submicron-sized (~180 ± 50 nm) grains and a few planar defects (twins). Though the twins can significantly enhance the strength and SRS (Christian and Mahajan, 1995; Lu et al., 2005, 2009a,b), their effect can be neglected since the amount of twins is extremely low (statistically, only one even no twinned grain exists in a ϕ = 500 nm MC Cu pillar). No significant dislocations are observed in the submicron-sized Cu grains. In contrast, the cross-sectional TEM micrographs of ~2 μm-thick Cu thin films show a relatively higher density of dislocations in the top and bottom of the ⟨100⟩-SC Cu micropillars, as shown in Fig. 1(c) and (d) clearly.

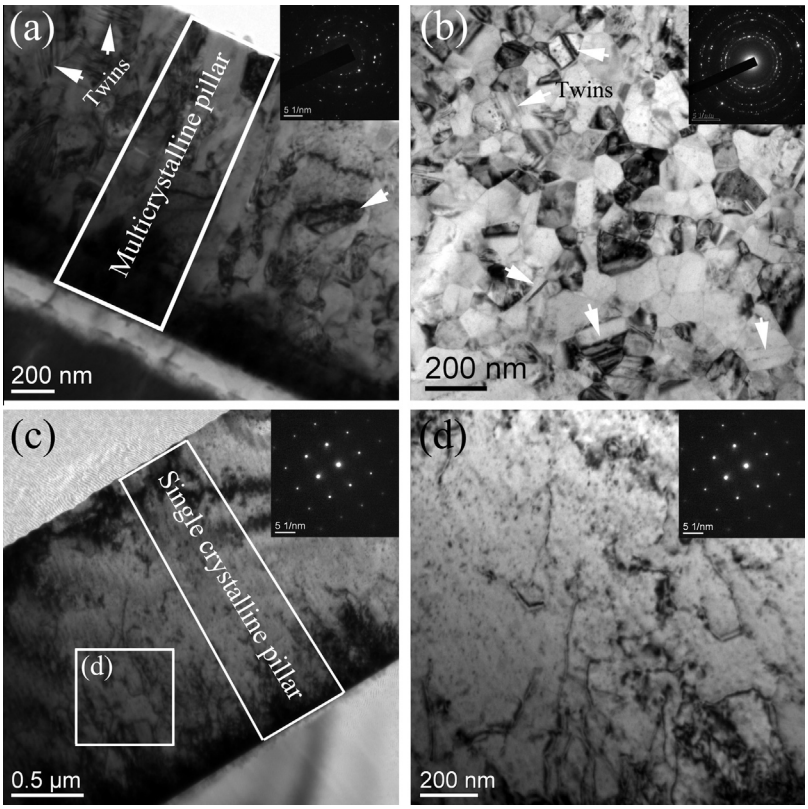

Fig. 1. Bright-field (a) cross-sectional and (b) planar TEM micrograph showing the microstructure of the MC Cu thin films; (c) bright-field cross-sectional TEM micrograph showing the microstructure of the ⟨100⟩-SC Cu films; (d) magnified TEM view of boxed area in (c) showing dislocation structure. Inset is the corresponding selected area diffraction patterns (SADPs). The white lines schematically showing the configurations of (a) ϕ = 500 nm MC and (b) ϕ = 600 nm ⟨100⟩-SC Cu pillars, respectively, the white arrows indicating the growth twins.

3.2. Deformation morphologies of MC/SC Cu pillars

Fig. 2(a)–(f) compares the SEM images taken before and after the uniaxial compression of the ((a) and (b)) ϕ = 500 nm, ((c) and (d)) ϕ = 800 nm and ((e) and (f)) ϕ = 1200 nm MC pillars at $\dot{\varepsilon} = 2 \times 10^{-4}$/s. It appears that all of the MC Cu pillars uniformly deform and exhibit significant barreling of the samples, comparable to what would be expected for macroscopic polycrystalline materials.

Fig. 3(a)–(f) shows the SEM images of the ((a) and (b)) ϕ = 600 nm, ((c) and (d)) ϕ = 800 nm and ((e) and (f)) ϕ = 1200 nm ⟨100⟩-SC pillars taken before and after the uniaxial compression at $\dot{\varepsilon} = 2 \times 10^{-4}$/s. In general, the samples with $\phi \sim 600$ nm are prone to deform in the quasi-single-slip mode, while samples with $\phi \sim 1200$ nm exclusively exhibit a bulk-like multiple slip deformation accompanied by significant barreling. The alternating slip deformation is readily occurred in intermediate sized samples with $\phi \sim 800$ nm. Furthermore, the deformation of the smallest ⟨100⟩-SC pillar by dislocation slip is mainly confined to the sample top, despite the symmetrical slip orientation, and limited to only one set of slip planes, see Fig. 3(b). The SC pillars deform along the single-slip-{111} plane accompanied with mild barreling radically different from those of observed in poly/multi-crystals and bicrystals (Kunz et al., 2011). It should be pointed out that the deformation morphologies of the present two types of Cu pillars are $\dot{\varepsilon}$-independent within this limited data set.

3.3. Strain rate effect on stress–strain response in MC/SC Cu pillars

Figs. 4 and 5 present the true stress–strain response of MC and ⟨100⟩-SC Cu pillars at different strain rates (Figs. 4 and 5(a)) and different diameters (Figs. 4 and 5(b)), respectively. All of the true stress–strain curves are characterized by a nearly elastic loading followed by multiple intermittent strain bursts with size ε_b, as schematically shown in Figs. 4 and 5. It is noticeable that in these true stress–strain curves there is a gradual transition from elastic to plastic deformation and relatively little strain hardening across all the pillars tested. To analyze the discrete nature of stress–strain response, we employ a two-point forward-Euler time differentiation of the displacement signal (Brinckmann et al., 2008; Jennings et al., 2011; Friedman et al., 2012). Following the approach of Dimiduk et al. (2006), Csikor et al. (2007), the displacement rate shows

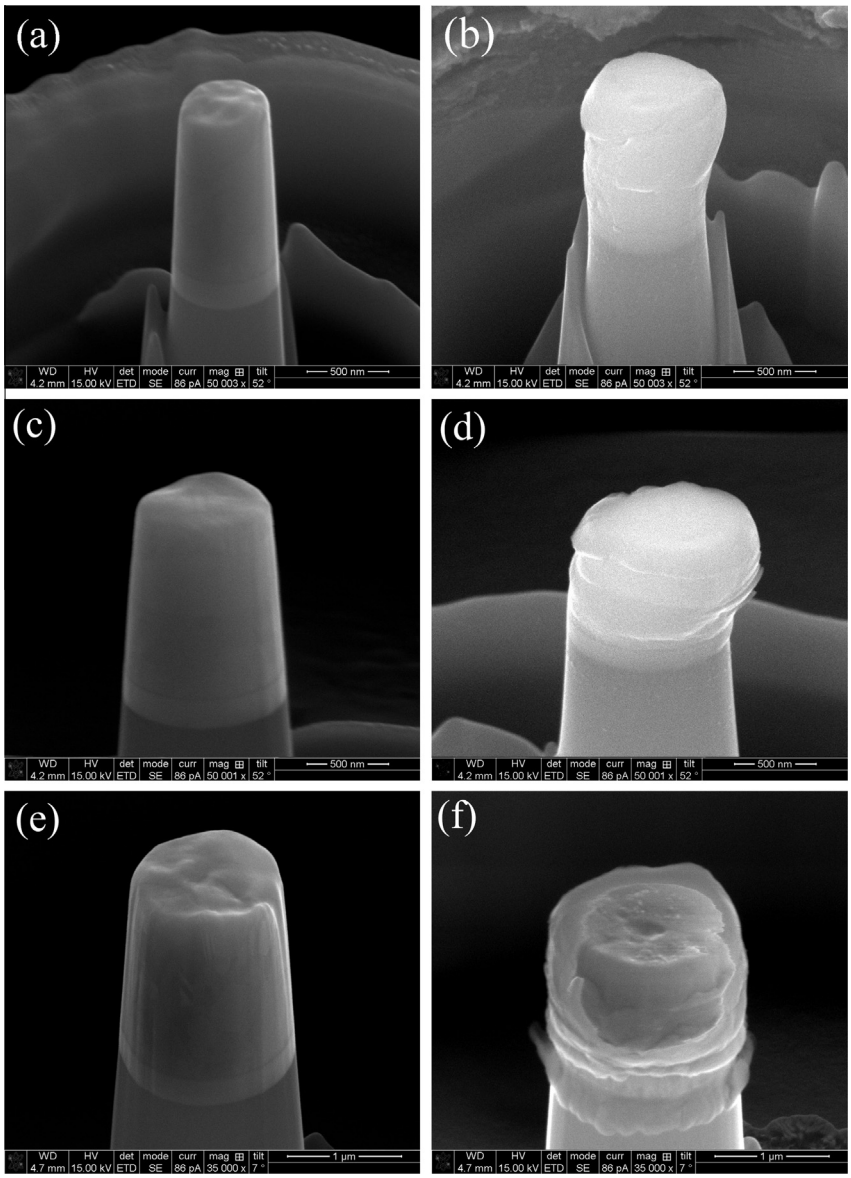

Fig. 2. Typical SEM images of the MC Cu micropillars before and after the uniaxial compression tests. As milled (a) ϕ = 500 nm, (c) ϕ = 800 nm and (e) ϕ = 1200 nm MC Cu pillar; compressed (b) ϕ = 500 nm, (d) ϕ = 800 nm and (f) ϕ = 1200 nm MC Cu pillar showing barreling of the micropillar.

distinct displacement bursts intermitted by periods of continuous deformation. It is found in Fig. 4 that the strain bursts are significantly suppressed due to the presence of GBs in the MC Cu pillars, fundamentally different from the ⟨100⟩-SC Cu samples (see Fig. 5). Furthermore, the higher $\dot{\varepsilon}$, the fewer and smaller bursts in ϕ = 500 nm MC Cu pillars (Fig. 4(a)), contrary to that of ϕ = 600 nm SC pillars (Fig. 5(a)). The greater is the ϕ, the smoother is the plastic flow of MC Cu pillars, as shown in Fig. 4(b). This is similar to that of ⟨100⟩-SC Cu pillars (see Fig. 5(b)). In other words, the faster $\dot{\varepsilon}$ and larger ϕ can lead to smoother stress–strain curves in the present MC Cu pillars. In contrast, the SC Cu pillars exhibit that the faster $\dot{\varepsilon}$ results in catastrophic strain bursts as opposed to the multiple successive bursts characteristic at slower $\dot{\varepsilon}$, while the greater ϕ leads to smoother plastic flow. It also appears that the flow stress (σ) strongly depends on $\dot{\varepsilon}$ – and ϕ for both MC and SC Cu pillars, *i.e.*, higher $\dot{\varepsilon}$ and smaller ϕ results in higher σ.

3.4. The SRS in MC/SC Cu pillars

It is well known that the rate-limiting processes of a material can be characterized by two key kinetic signatures of deformation mechanism, *i.e.*, SRS (m) and activation volume (V^*) (Zhu et al., 2008; Gu et al., 2011). In a thermally activated process

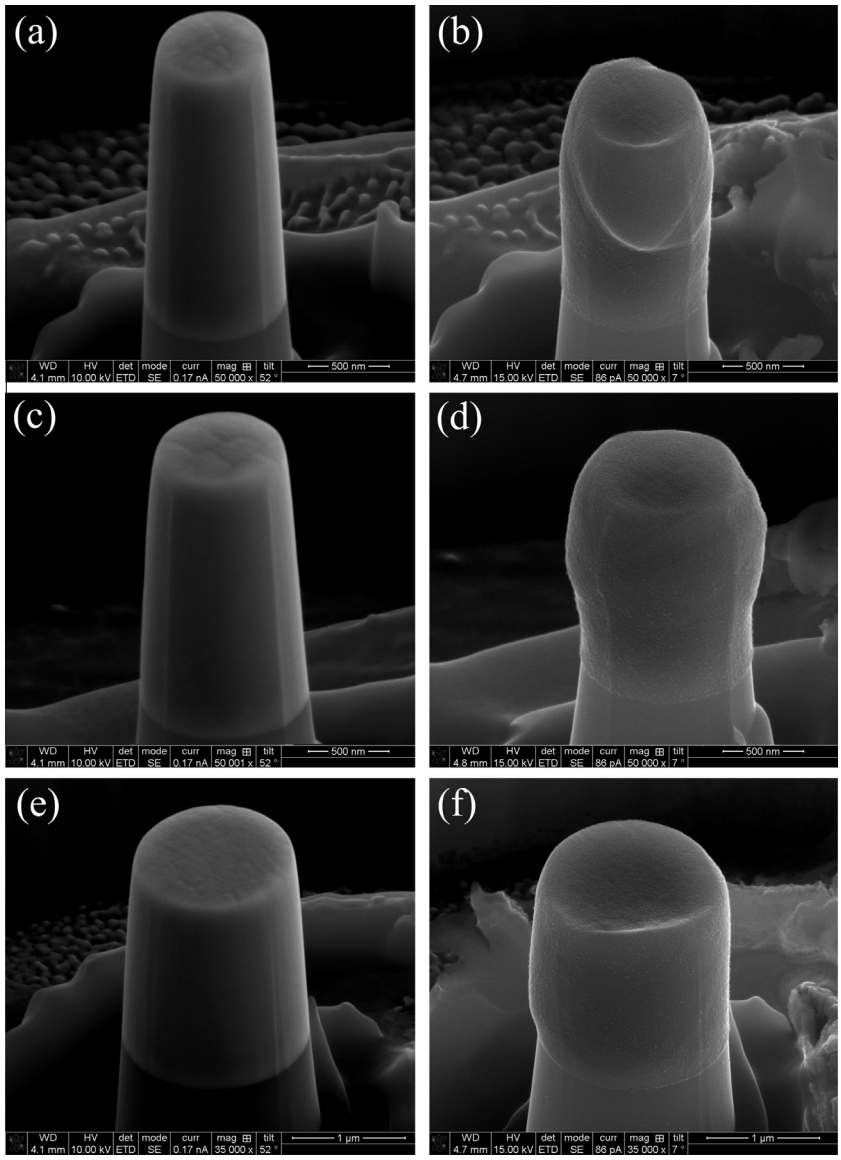

Fig. 3. Typical SEM images of the ⟨1 0 0⟩-SC Cu micropillars before and after the uniaxial compression tests. As milled (a) ϕ = 600 nm, (c) ϕ = 800 nm and (e) ϕ = 1200 nm MC Cu pillar; (b) ϕ = 600 nm ⟨1 0 0⟩-SC Cu pillar after compression showing single-slip deformation, (d) ϕ = 800 nm and (f) ϕ = 1200 nm ⟨1 0 0⟩-SC Cu pillar after compression showing multiple-slip deformation.

that triggers considerable plastic flow, the V^* is defined using the change of $\dot{\varepsilon}$ with respect to the flow stress σ, the absolute temperature T and the Boltzmann constant k_B as (Gu et al., 2011)

$$V^* = \frac{\sqrt{3}k_B T}{\sigma}\frac{\partial \ln(\dot{\varepsilon})}{\partial \ln(\sigma)}. \tag{3}$$

The SRS m is related to the activation volume V^* by the following expression

$$m = \frac{\sqrt{3}k_B T}{V^*\sigma} = \frac{\partial \ln(\sigma)}{\partial \ln(\dot{\varepsilon})}. \tag{4}$$

We determined the SRS m and activation volume V^* for all of our compression tests at different strain rates, spanning over two orders of magnitude. In SC pillars, such as Cu (Kiener and Minor, 2011a,b; Kiener et al., 2011), Ni (Frick et al., 2008) and Au (Maaß et al., 2009), transition from ordinary forest hardening to exhaustion hardening or starvation hardening can alter the values of strength power-law exponent (n). In other words, once dislocation substructures evolve with plastic strain ε_p

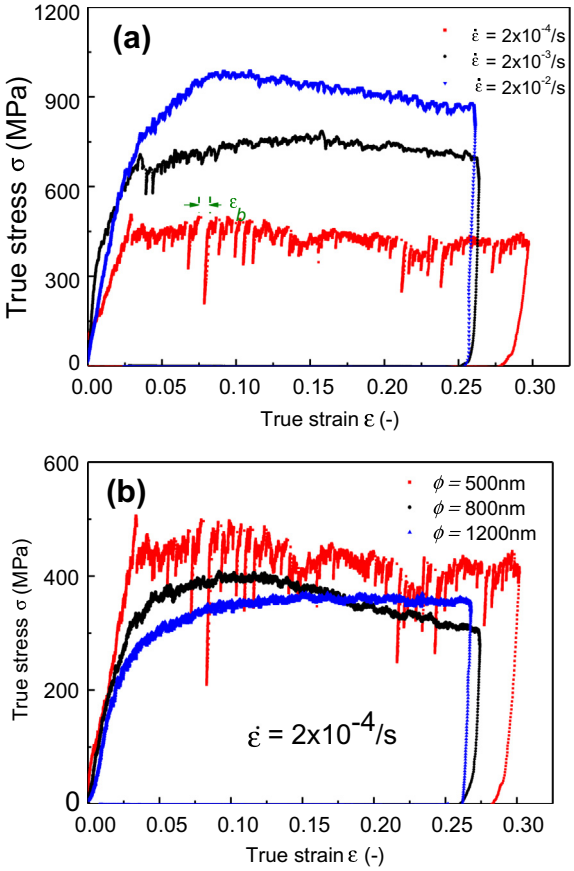

Fig. 4. True stress–strain plots for the (a) ϕ = 500 nm MC at different strain rates and (b) three different ϕ = 500, 800 and 1200 nm MC Cu micropillars compressed at strain rate 2×10^{-4}/s.

(or $\dot{\varepsilon}$), the deformation mechanisms will also evolve with ε_p (or $\dot{\varepsilon}$). In this regard, the choice of characteristic strength should be carefully considered. Because large stress–strain scatter is generally observed in the initial stage of plastic flow in a micro-compression test (probably caused by the rough tip of the pillar/indenter), the flow stress at a relative large amount of strain (ε_p = 2.5%) is chosen to be discussed here, following the spirit of previous studies (Dimiduk et al., 2005; Maaß et al., 2009; Schneider et al., 2009a, 2011; Maaß and Uchic, 2012; Zhang et al., 2012a). In addition, to verify the evolution of dislocation substructures with plastic strain and the potential strain hardening behavior in the submicron and micron-sized pillars, the maximum strength (at $\varepsilon_p \approx 5\%$) was also selected to discuss the $\dot{\varepsilon}$-effect on the mechanical response of MC and SC pillars. The experimental data for the strength ($\sigma_{2.5}$) at plastic strain ε_p = 2.5% and the maximum strength (σ_{max}, at $\varepsilon_p \approx 5\%$) as a function of $\dot{\varepsilon}$ are shown on a log–log plot in Fig. 6(a). It is found that the strengths of present two types of pillars that behave in a "smaller is stronger" fashion (see Fig. 6(b)) increase with increasing $\dot{\varepsilon}$, as is consistent with other reported results (Meyers et al., 2006; Jennings et al., 2011). Particularly, the MC Cu pillar show a much higher strength than the ⟨1 0 0⟩-SC Cu pillar at an equivalent ϕ, as shown in Fig. 6(b).

In Fig. 7(a), the m values are 0.147–0.178 and 0.023–0.025 for the smallest MC and SC pillars, respectively, which generally decrease with increasing ε_p and are much greater than that of bulk SC Cu pillars ($m \sim 0.006$ (Chen et al., 2006)). It appears that at a constant ε_p, the SRS m for both MC and SC pillars monotonically increases with reduction in ϕ. Interestingly, the SRS m is the smallest for bulk polycrystalline Cu (Wei et al., 2004; Chen et al., 2006), then the ϕ = 1200 nm MC Cu, followed by the ϕ = 500 nm MC Cu pillars in ascending sequence. This is worthy of being studied deeply, which is beyond the scope of present work. In general, it is possible to gain insights into the microstructural plasticity mechanisms responsible for this surprising high SRS in MC pillars by analyzing the activation volume. Notably, the V^* determined here is about $\sim 4b^3 - 5b^3$ for ϕ = 500 nm MC Cu pillars and slightly increases to $\sim 11b^3 - 13b^3$ at ϕ = 1200 nm. However, the V^* of SC Cu pillars increases from $\sim 50b^3 - 60b^3$ to $\sim 130b^3 - 140b^3$ with increasing ϕ from 600 to 1200 nm. For comparison and completeness, the ranges of V^* determined for ⟨1 1 1⟩-SC pillars (Jennings et al., 2011) and polycrystalline Cu (Chen et al., 2006) are also plotted in Fig. 7(b).

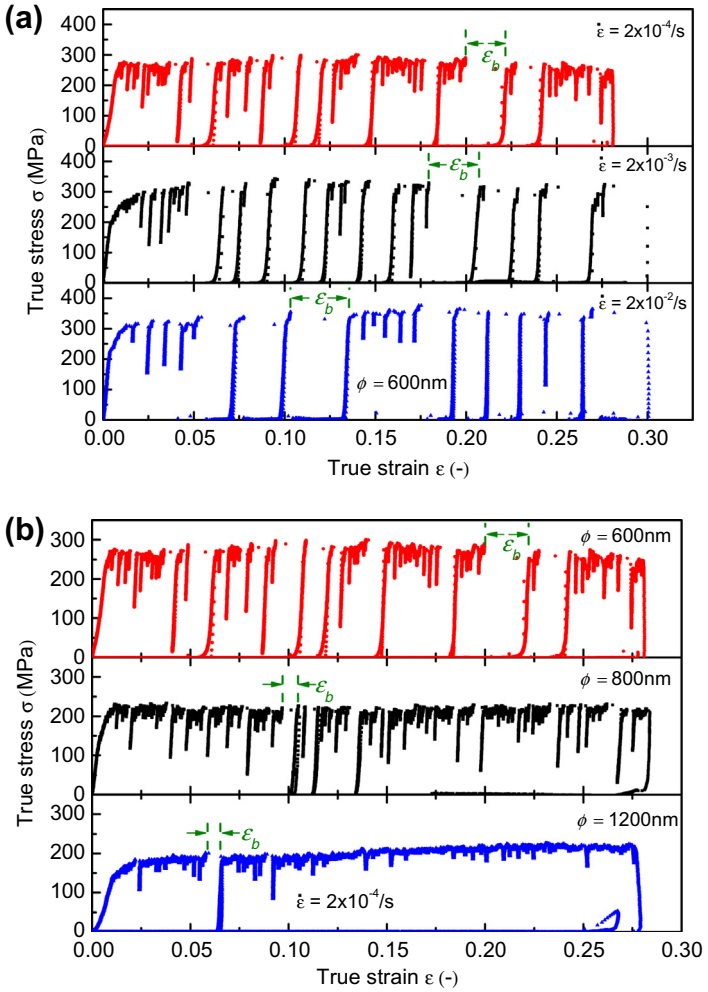

Fig. 5. True stress–strain plots for the (a) $\phi = 600$ nm ⟨100⟩-SC at different strain rates and (b) three different $\phi = 600$, 800 and 1200 nm ⟨100⟩-SC Cu micropillars compressed at strain rate 2×10^{-4}/s.

4. Discussion

4.1. Internal structure features related deformation mechanism: dislocation-mediated mechanism versus GB-mediated mechanism

4.1.1. Effects of grain size/GBs on strength of MC pillars: strengthening versus weakening

In bulk ultrafine-crystalline (with $d \sim 100$–1000 nm) metals, GBs obscure the passage of the gliding dislocations nucleated from GBs, thereby elevating their crystalline strengths (Cheng et al., 2003; Zhang et al., 2010, 2012d). Due to the strong constraining effects of neighboring grains, the GB-mediated processes like GB sliding and grain rotation are difficult to switch on in samples with submicron-sized grains (Schiotz and Jacobsen, 2003; Shan et al., 2004). As observed in Fig. 6, the σ_{max} of MC pillar is much higher than that of ⟨100⟩-SC pillar at an equivalent ϕ and a given $\dot{\varepsilon}$. This is mainly because (i) the compatibility condition at the GBs applies additional constraints to the deformation; and (ii) the GBs hinder dislocation motion (Jang et al., 2011). However, Jang and coworkers (Jang et al., 2011) have unveiled that the GB-mediated processes in lieu of dislocation-driven processes operate in electroplated $\phi = 500$ nm MC Cu pillars with $d \sim 160$ nm, due to the weak constraining effects of free side surface. The fundamental difference between present MC pillars ($d \sim 180$ nm) and electroplated ones ($d \sim 160$ nm) can be attributed to the influences of microstructure and orientation (Jang et al., 2011). The marked increase in strength of MC pillar with reduction in sample size stems from the reduced length of dislocation source, which needs a higher stress to be activated (Rinaldi et al., 2008). Similar observations have been reported in nanocrystalline ($d \sim 30$ nm) Ni pillars (Rinaldi et al., 2008) and nanolayered Cu/Zr pillars (Zhang et al., 2012a). Specifically, present authors (Zhang et al., 2013) have revealed the deformation crossover from strengthening to weakening in nanocrystalline Zr pillars with reducing ϕ, owing to the operation of GB-mediated processes at a larger $d \sim 35$ nm than the critical $d \sim 15$ nm. As such, two competing processes may emerge simultaneously upon the introduction of internal GBs into smaller

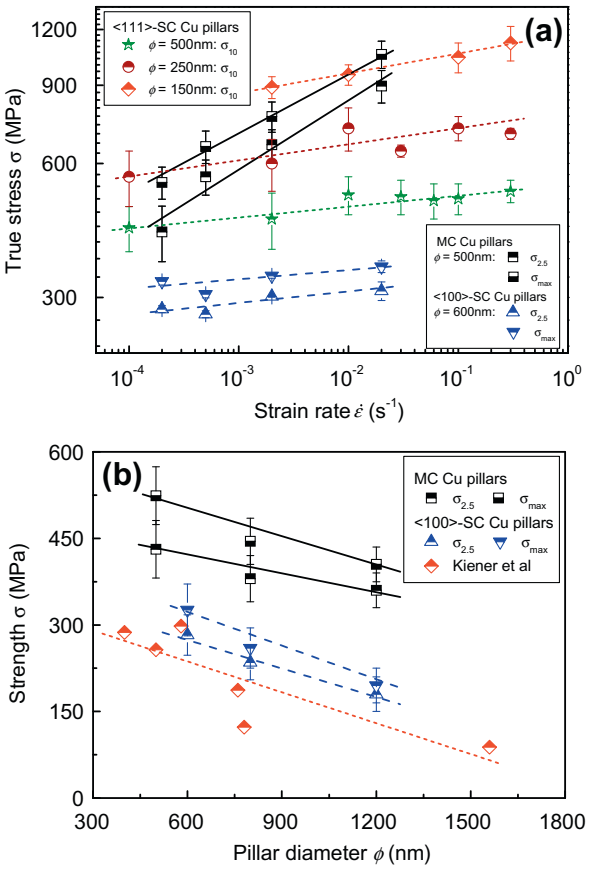

Fig. 6. (a) The strengths $\sigma_{2.5}$ and σ_{max} of MC pillars (ϕ = 500 nm) and ⟨100⟩-SC Cu pillars (ϕ = 600 nm) as a function of $\dot{\varepsilon}$. The strength σ_{10} of ⟨111⟩-SC Cu pillars (Jennings et al., 2011) with three different diameters is also plotted for comparison (b) The strengths $\sigma_{2.5}$ and σ_{max} of MC and ⟨100⟩-SC Cu pillars as a function of ϕ at $\dot{\varepsilon} = 2 \times 10^{-4}$/s. The yield strength ⟨100⟩-SC Cu pillars with $\eta > 5$ at $\dot{\varepsilon} = 5 \times 10^{-3}$/s (Kiener and Minor, 2011b) is also plotted for comparison (red half diamond). (For interpretation of the references to colour in this figure legend, the reader is referred to the web version of this article.)

($\eta < 3$) MC nanopillars: Hall–Petch-like strengthening and GB-mediated weakening. Whether the small aspect ratios (<2) affect the measured strengths of MC pillars, at least to what degree, is worthy of a separate study that is out of the scope of present work. On the other hand, the SRS m (~0.1–0.18) of the present MC pillars is still far less than that of caused by GB-mediated deformation (~0.5) (Meyers et al., 2006), indicative of dislocation-mediated mechanism dominates the plastic deformation.

4.1.2. Effects of initial dislocation substructure and slip geometry on deformation of SC pillars

Recent experimental findings have shown that it is the initial dislocation density rather than the fabrication technique that drives the size effect in fcc metals (Bei et al., 2008; Rao et al., 2008; Jennings et al., 2010, 2011; El-Awady et al., 2013; Schneider et al., 2013). In Fig. 1(c) and (d), a very high density of dislocations is respectively observed near the top and bottom ends of the SC Cu samples. This is because during the deposition process, the formation of (threading) dislocations can be an effective way to release the thermal stress caused by the mismatch between the substrate and Cu film (Dehm et al., 2001; Inkson et al., 2002; Dehm et al., 2003). Once the threading dislocations (or the segment of dislocations) with opposite sign collide with each other during the film growth, they can annihilate (LeGoues, 1994). Thus, a lower density of dislocations is observed in the middle, while a higher density of dislocations is respectively observed neighboring the substrate and top in such a "single crystal-like" thin film.

For the present ⟨100⟩-SC pillars, the pre-existing dislocations are difficult to be mechanically annealed (Shan et al., 2008; Zhou et al., 2011). Instead, the reconstruction of jammed dislocation network plays a crucial role in exhaustion hardening and creating new dislocation sources (Csikor et al., 2007; Rao et al., 2008; Kiener and Minor, 2011b; Zhou et al., 2011; Wang et al., 2012) in deformation. As deformation proceeds, dislocations move downwards and finally accumulate at the bottom of SC Cu pillars, similar to other reported deformed SC Cu (Kiener and Minor, 2011b), Ni (Frick et al., 2008; Shan et al., 2008) and Al (Wang et al., 2012) pillars. It is further reported that smaller SC pillars exhibit a reduction in their strength with increasing dislocation density while larger pillars exhibit an increase in strength (Rao et al., 2008; El-Awady et al., 2013; Schneider et al., 2013). Also, the size of SC crystal at which the transition of increase-to-reduction in strength emerges, increases with

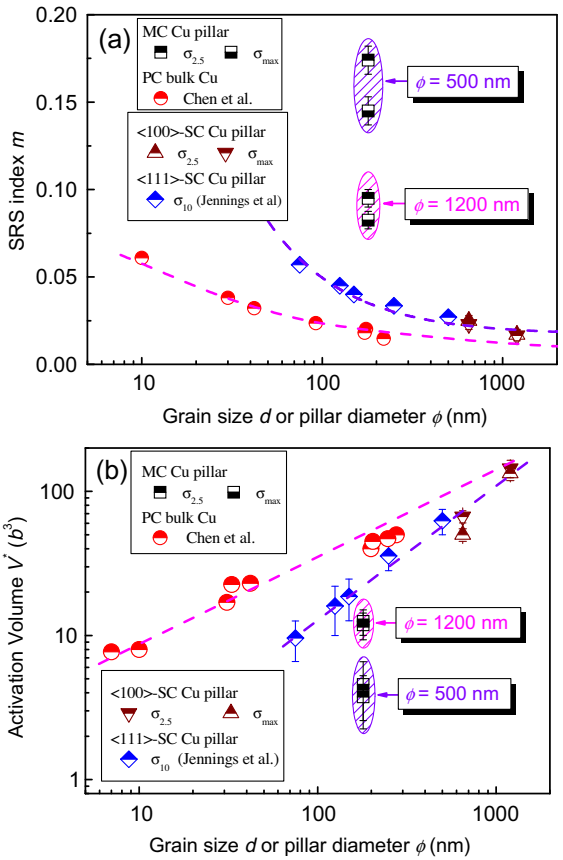

Fig. 7. (a) The SRS index m of MC and ⟨100⟩-SC Cu pillars at two different strains and ⟨111⟩-SC Cu pillars (Jennings et al., 2011) as a function of ϕ and that of bulk polycrystalline Cu (Wei et al., 2004; Chen et al., 2006) as a function of d. (b) The activation volumes of MC and ⟨100⟩-SC Cu pillars at two different strains and ⟨111⟩-SC Cu pillars (Jennings et al., 2011) as a function of ϕ and those of bulk polycrystalline Cu (Chen et al., 2006) as a function of d. The dash lines are visual guide.

decreasing dislocation density (Rao et al., 2008; El-Awady et al., 2013; Schneider et al., 2013). In the present case, a high dislocation density renders SC pillars yield at low mechanical stress and the deformation is relatively continuous and uniform (reflected by the small-sized bursts). This sharply contrasts with the smaller pillars with low dislocation density characterized by explosive deformation leading to a sudden change in the pillar geometry (Xie et al., 2013). Kiener and coworkers (Kiener et al., 2008, 2009a) have proved that for aspect ratios greater than 2 there is no pronounced impact of the aspect ratio on the flow stress, below which a clear increase in the flow stress associated with a suppression of distinct load drops is observed. Therefore, in present work the smallest aspect ratio (~1.7) likely contributes to the measured strength and smoothes the true stress–strain curves in the largest SC pillars.

The inevitable taper and top rounding when fabricating pillars using annular milling can lead to higher stresses at the sample top, which renders the deformation always starts at the sample top. This is further amplified by the friction between diamond and specimen top, resulting in a multiaxial stress state which promotes dislocation nucleation (Kiener et al., 2009b). Other important factors are misalignment and lateral stiffness of the system. The main effect of misalignment is a reduction of the linear loading slope (Raabe et al., 2007), which does not affect our data for evaluation of the yield strength (Kiener and Minor, 2011b). Moreover, we observe close agreement between loading and unloading slope (see Figs. 4 and 5), indicating good alignment. Our present results indicate that smaller SC Cu pillars prefer to deform via single slip, while larger ⟨100⟩-SC Cu pillars are inclined to deform via multiple slip. In particular, small aspect ratios can render that multiple slip systems are activated even though the crystal is in single-slip orientation (Senger et al., 2011). At the interval range, the ⟨100⟩-SC Cu pillars tend to deform via alternating slip. Similar results were observed by Kiener and Minor in ⟨100⟩-SC Cu pillars with greater aspect ratios >5 (Kiener and Minor, 2011b). The deformation morphologies observed for the different sample sizes suggest that the deformation behavior is source-limited (Kiener and Minor, 2011b). Smaller samples, albeit being oriented for multiple slip, deform like single-slip-oriented crystals due to the limited number of dislocation sources in the sample volume. The larger the samples, the more closely the observed deformation behavior comes to what is known from bulk Cu with a ⟨100⟩-orientation. This source-limited situation might become even more pronounced due to the tapered geometry of the pillars, as this creates a stress gradient over the sample height, thereby confining the actual deforming

volume further (Kiener et al., 2009b). Ideally, there is no strain hardening effect for single slip-plane flow in defect-free fcc samples. Indeed, our microtestings indicated that the multiple slip did not significantly contribute to the hardening behavior, as is consistent with both the experimental findings in submicron-sized SC Mo and Nb pillars (Schneider et al., 2009a, 2011) and the 3D-DDD simulation results (Senger et al., 2011). This is probably caused by the existence of dislocations rather than the dislocation-starved state of the samples. Note that the distribution of avalanches strains is insensitive to the presence of single or multiple slip systems and even to the activation of cross slip, indicating university with respect to slip geometry (Csikor et al., 2007).

4.2. Strain burst behavior of MC/SC pillars: strain rate effect versus grain/pillar size effect

4.2.1. The origin of strain burst: dislocation avalanches versus mechanical annealing

Our present results have unambiguously verified that in the MC pillars, GBs hinder the propagation of dislocation avalanches, and thus sizes of strain bursts should be reduced by a factor of $\sim\eta^{-2}$ compared with the SC pillars at an equivalent sample size (Csikor et al., 2007). Recent in situ TEM compression testing of submicron-sized Al pillars showed two sample size regimes with contrasting behavior underlying the large strain bursts (Wang et al., 2012). For smaller pillars, the strain bursts originate from explosive and highly correlated dislocation generation, characterized by very high collapse stresses and nearly dislocation-free post-collapse microstructure (mechanical annealing (Shan et al., 2008)), while for larger pillars, the strain bursts result from the reconstruction of jammed dislocation configurations, featuring relative low stress levels and retention of dislocation network after bursts (Wang et al., 2012).

In our case, the small $V^* \sim 4b^3 - 13b^3$ indicates that dislocations emitted from the boundaries are required to sustain deformation of present MC Cu pillars (Zhu et al., 2008; Jennings et al., 2011). As such, pre-existing dislocations are perhaps mechanically annealed and the jammed dislocation configurations cannot form during subsequent straining, similar to the small-sized (ϕ < 200 nm) SC Cu (Kiener and Minor, 2011b), Ni (Shan et al., 2008), Al (Wang et al., 2012) and Mo (Huang et al., 2011) pillars, which depends sensitively on the strain rates (discussed below). In contrast, the ⟨100⟩-SC Cu pillars have large $V^* \sim 50b^3 - 140b^3$ and a high density of dislocations. This renders the strain bursts occur at a relatively lower stress and the simulation-predicted dislocation avalanche picture appears relevant, where reconstruction of jammed dislocation network plays a dominant role in SC pillars (Dimiduk et al., 2006; Csikor et al., 2007; Norfleet et al., 2008; Shan et al., 2008; Huang et al., 2011; Wang et al., 2012).

4.2.2. The model of statistical absorption of dislocations by GBs

Recent experimental results (Rajagopalan et al., 2010; Mompiou et al., 2012) have uncovered that as d decreases down to ~1500 nm, the dislocations emitted from (bulk and/or boundary) sources can traverse the grain interior and be absorbed by GBs or just only stay in grain interior, similar to the molecular dynamic simulation results (Yamakov et al., 2004; Van Swygenhoven et al., 2006). On the basis of these findings, Carlton and Ferreira (Carlton and Ferreira, 2007) proposed a model of statistical absorption of dislocations by GBs (called SAD model hereafter) applicable in nanostructured materials to make some interesting and useful predictions about the effects of GBs strengthening related to strain rate (Huang et al., 2010), temperature (Farrokh and Khan, 2009) and activation energy (GB structure).

Following the sprit of Carlton and Ferreira (Carlton and Ferreira, 2007), we attempt to semi-quantitatively explain the size and strain rate dependent burst behaviors by envisioning the following three scenarios: (i) For the pristine and low dislocation density samples, the mobile dislocations emitted from (bulk and/or boundary) sources can either traverse the pillar and fully/partly insert in the GBs, or escape from the free surface at present studied length scale; (ii) For the samples with heterogeneous dislocation distribution, the high dislocation density zone can be regarded as a GB, since dislocation interactions in such zone can probably form immobile dislocation tangles/junctions or annihilate each other. Here, we consider the SC Cu pillar as a composite material, consisting of soft zone (with a low dislocation density) and hard zone (with a high dislocation density), as detailed in Ref. (Mughrabi, 1983) for a heterogeneous dislocation distribution to interpret single-slip and multiple-slip deformation, then it follows naturally that soft and hard zones are respectively subjected to backward and forward internal stresses. The dislocation mean free path (λ) thus is shorter in the present ⟨100⟩-SC pillars with respect to the corresponding pristine SC pillars (Mompiou et al., 2012); and (iii) The pre-existing and newly generated immobile dislocations (including dislocation jams/junctions *etc*) can be transformed into mobile dislocations, absorbed by GBs and/or annihilated at free surface, once the strain burst occurs. Therefore, according to the SAD model (Carlton and Ferreira, 2007), the probability of a dislocation being absorbed by the GBs, P_{dis}, can be expressed by:

$$P_{\mathrm{dis}} = \left[1-(1-p)^{N}\right]^{J} = \left\{1-\left[1-\exp\left(\frac{-\left(\Delta G+\tau_0 b^3\right)}{k_{\mathrm{B}}T}\right)\right]^{\frac{sb\nu}{\dot{\varepsilon}d}}\right\}^{\omega l}, \tag{5}$$

where $p = \exp[-(\Delta G + \tau_0 b^3)/(k_{\mathrm{B}}T)]$ is the probability of an atom successfully jumping into the GB/surface in a single attempt; $N = (sb\nu)/(\dot{\varepsilon}d)$ is the number of attempted jumps by dislocation core atoms to the GB/surface during a given time; $J = \omega l$ is the total number of atoms on the dislocation core jumping into the GB, where the dislocations length l is proportional to d or ϕ; ΔG is the activation energy for atomic migration (or dislocation nucleation), varying within the range of ~0.6–0.95 eV (Carlton and Ferreira, 2007; Jennings et al., 2011), and is a decreasing function of the effective stress (or proportional to

the characteristic size d or ϕ) (Conrad, 2003; Jiang et al., 2004); $k_B = 1.38 \times 10^{-23}$ J/K is Boltzmann's constant; T is temperature; $\dot{\varepsilon}$ is strain rate; v is Debye frequency; τ_0 is resolved shear stress; ω physically corresponds to a the atomic linear density of the dislocation core and is independent of d or ϕ; and other symbols have the same meaning as above. The case $P_{dis} = 1$ means GBs are transparent and do not take part in strengthening but rather would soften the materials. In contrast, $P_{dis} = 0$ implies that GBs are opaque and can inhibit mobile dislocations traverse the GB, thereby strengthening the materials. By using $\tau_0 = s\sigma_0 = 10$ MPa, $b = 0.2556$ nm, $T = 300$ K, $v = 7.2 \times 10^{12}$ Hz, $l = d$, $\omega = 6.5$ atoms/nm, and Eq. (5), we found that d for $P_{dis} = 0$ monotonically increases from 8 to 250 nm with reducing $\dot{\varepsilon}$ from 2×10^{-2} to 2×10^{-4}/s, see Fig. 8(a) with $\Delta G = 0.73$ eV. The probability P_{dis} as a function of d at different activation energies and at $\dot{\varepsilon} = 2 \times 10^{-4}$/s is plotted in Fig. 8(b), from which one can see that the lower ΔG, the larger d for $P_{dis} = 0$.

For the MC Cu pillars, upon loading, the dislocations can nucleate from the ledges located at GBs (Li and Chou, 1970; Spearot et al., 2007). When a grain deforms at higher $\dot{\varepsilon}$ with smaller P_{dis}, more emitted dislocations partly insert in or pile-up against the opposite GB per unit time. This process provides insufficient time for absorption of dislocations and subsequently induces the ready-to-go dislocations (partly/completely) stay in grain interior. It generates a fairly larger stress field and causes a more rapid and higher repulsive stress concentration at GBs, hindering the dislocations nucleation. Indeed, as pointed out by Mompiou et al. (2012), although individual dislocations dissolve in GBs in a few tens of seconds, or in a few minutes, their long-range stress fields should remain sufficient to repel other following (non-screw) dislocations. However, at lower $\dot{\varepsilon}$, higher P_{dis} means the absorption process is easier to operate. It results in less accumulation of dislocation in grain interior and a lower back stress, facilitating the subsequent emission and absorption of mobile dislocations (Mompiou et al., 2012). Additionally, P_{dis} strongly depends on the characteristic size of pillars, such as d. The larger d, the lower P_{dis}. The competing effects between these two factors contribute to the observed burst behaviors in MC pillars.

In sharp contrast with MC pillars, the SC pillars exhibit larger strain burst sizes at higher $\dot{\varepsilon}$. This agrees well with the most recent findings in ⟨1 1 1⟩-SC Cu, ⟨1 0 0⟩-SC Mo and Au pillars (Jennings et al., 2011; Friedman et al., 2012). It also appears that avalanches strains or burst sizes decrease in inverse proportion to sample size in present studied $\dot{\varepsilon}$ range, as is consistent with the experimental observations in SC Ni (Uchic et al., 2004; Dimiduk et al., 2005; Frick et al., 2008), Au (Brinckmann et al., 2008; Kim and Greer, 2009) and Mo (Kim and Greer, 2009; Schneider et al., 2009b; Kim et al., 2010) and the 3D-DDD simulations (Csikor et al., 2007). These results can be reconciled by considering the dislocation nucleation and accumulation

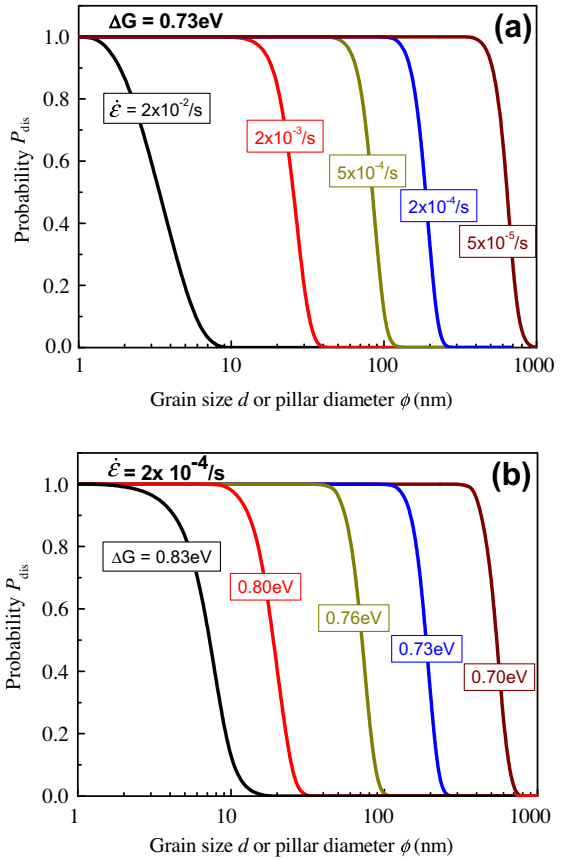

Fig. 8. The probability P_{dis} of dislocation absorbed by GBs as a function of d or ϕ at different (a) strain rates and (b) activation energies.

in light of the SAD model as well. In SC Cu pillars, most of dislocations nucleated from internal sources as well as the pre-existing mobile dislocations run across the pillar and may be hindered by the pre-existing pinning sites instead of escaping from the surface ($P_{dis} \approx 0$) at whole $\dot{\varepsilon}$ range, especially at a low stress level. The higher is the $\dot{\varepsilon}$, the more dislocations pile-up against the barrier, and the lower is the probability of dislocation annihilate at surface (or lower P_{dis}). Therefore, the dislocation pile-ups will induce large stress concentrations, inhibiting further dislocation emission and motion. When the increased external stress is large enough, overwhelming the internal repulsive stress or the barrier of dislocation jams/junctions, more stored dislocations can continue to move forward and probably annihilate at surface. This renders a larger sized strain burst observed in the stress–strain curves at higher $\dot{\varepsilon}$. It also explains that faster $\dot{\varepsilon}$ compressions result in one catastrophic strain burst, opposite to the multiple successive bursts characteristic at a slower $\dot{\varepsilon}$. On the other hand, for a given $\dot{\varepsilon}$, the lager is the ϕ, the greater is λ and the lower is the likelihood for the occurrence of dislocation avalanches and reconstructions (also lower P_{dis}). It is the root cause for the bulk single crystals exhibit smoother stress–strain plots, while the small sized SC pillars show multiple discrete strain bursts, as seen in Fig. 5.

It should be pointed out that this model does not include the effect of dislocation pile-ups (and dislocations of fully/partly inserted GBs) in larger grains for MC pillars, especially for SC pillars. In MC pillars, even if these repeated absorption processes can change the GB structures and generate corresponding stress fields, the influence of stress fields on the following mobile dislocations depends on the dislocation nature *i.e.*, non-screw and screw (Bitzek et al., 2008; Mompiou et al., 2012). The more non-screw dislocation pile-ups are, the higher stress concentration is. This will lower the contribution of related thermal activation processes, rendering lower ΔG is needed. Also, it will hinder further dislocation nucleation and emission, resulting that a higher applied stress is required to generate one dislocation. Nevertheless, the cross-slipping screw dislocations reach GBs at different places, leading to weak stress concentrations, thereby the following approaching dislocations can be absorbed by GBs (Mompiou et al., 2012). Unlike the MC samples where dislocations are blocked from leaving the sample by the GBs constraining effect, applied stress can drive dislocations escape from the surface of SC pillars, leaving a relative clear free path for dislocations that are activated later (Zhou et al., 2012). It thus reasonably assumes that ΔG for atomic migration in SC pillars is relatively lower.

Despite the simplicity of this model, the combination of our experimental findings and those predicted by the model indicates that absorption of dislocation by GBs strongly contribute to the size- and rate-dependent strain burst in MC/SC pillars. While, their discrepancies are probably caused by the SAD model does not take into account these factors, such as deformation-induced internal stresses and any extra thermal contributions from the nearby surface, which can affect ΔG.

4.3. Transition of hardening mechanisms: forest hardening versus starvation hardening

Another striking feature of the true stress–strain curves in Fig. 4 is the lack of hardening in MC pillars at low $\dot{\varepsilon}$, which suggests that the dislocations nucleated from the GBs/surface can run across the grain interior and be absorbed by and/or annihilate at GBs/surface totally, as discussed above. One of the consequences of dislocation starvation is that the internal microstructure should not appreciably change as a function of plastic strain, allowing the use of the flow stress at $\varepsilon_p = 2.5\%$, even at $\varepsilon_p = 5\%$ in estimation of rate-limiting processes (m or V^*) for MC Cu pillars. In contrast, at high $\dot{\varepsilon}$ the hardening phenomenon observed in MC pillars suggests the dislocation substructures indeed evolve with ε_p. That is to say, there exists the accumulation and interaction of dislocations (ordinary forest hardening) instead of starvation, which is partly supported by the large difference in m (e.g. $m \sim 0.147$ at $\sigma_{2.5}$, $m \sim 0.178$ at σ_{max} for $\phi = 500$ nm MC pillars). In addition, the higher m compared with the reported m for NC Cu and even for that of $\phi = 150$ nm $\langle 1\,1\,1\rangle$-SC Cu pillars (see Fig. 7(a)) also indicates more dislocation-GB interactions in MC pillars (Wei et al., 2004; Wei, 2007). This is probably caused by the combination of GBs and surface effects in these small-volume MC pillars with $\eta \sim 3$–7. On the other hand, in the present SC pillars, the strain as well as the $\dot{\varepsilon}$ -effect on the stress–strain response is negligible, as is verified by the almost identical m values ~0.024 (correspondingly, $V^* \sim 50b^3 - 60b^3$ for $\phi = 600$ nm SC pillars). The multiplication of internal dislocation sources should control the plastic flow with increasing ε_p (Zhou et al., 2011). Most recently, Jennings and coworkers (Jennings et al., 2011) studied the SRS of $\langle 1\,1\,1\rangle$-SC Cu pillars and revealed that SRS m increases from ~0.027 to ~0.057 with decreasing ϕ from 500 to 75 nm (correspondingly, V^* decreases from $62b^3$ to $9.6b^3$) at $\dot{\varepsilon} > 1 \times 10^{-1}$/s. Therefore, we can argue that introducing GBs can enhance the SRS of small-volume SC metals markedly.

The elevation of m in nanostructured metals has been reported before, such as for NC Ni (Schwaiger et al., 2003), NC Cu (Chen et al., 2006; Huang et al., 2010) and nanotwinned Cu (Lu et al., 2005; Dao et al., 2006). The rate/temperature dependence of the strength is normally attributed to the thermally activated process of overcoming of the obstacles to the motion of glissile dislocations. The SRS m can be related to the activation volume of the thermally activated event by Eq. (3). For fcc metals, the activation volume V^* can also be written as (Cheng et al., 2005)

$$V^* = b\chi l^*, \tag{6}$$

where b is the Burgers vector of the dislocations, χ is the distance (of the order of b) swept out by the mobile dislocation during one activation event, and l^* is the length of dislocation segment involved in the thermal activation (or the Friedel sampling length that scales with the average contact distance between two obstacles). Combining Eqs. (3) and (6) we get

$$m = \frac{\sqrt{3}k_B T}{\sigma V^*} = \frac{\sqrt{3}k_B T}{\sigma b \chi l^*}, \tag{7}$$

in which χ is approximately a constant. On the other hand, the strength has contributions from not only the dislocations but also the GBs, and it can be given as (Wei et al., 2004; Cheng et al., 2005)

$$\sigma = \sigma_0 + \alpha\sqrt{\rho} + \beta/\sqrt{d}, \tag{8}$$

where the first term accounts for the lattice friction, the second term arises from the Taylor equation, and the third term is due to the Hall–Petch relationship. α and β are proportionality factors. The obstacle spacing l^* can be viewed as having two possible limits, l_1^* and l_2^* (Cheng et al., 2005):

$$l_1^* = \xi/\sqrt{\rho}, \tag{9a}$$

$$l_2^* = \zeta d, \tag{9b}$$

where ξ and ζ are proportionality factors. l_1^* is the controlling length scale when the grain sizes and dislocation densities are both large (for the present SC pillars) such that dislocation density plays the dominant role. Neglecting the very small lattice friction term for fcc metals, the SRS index m can be expressed as

$$m = \frac{\sqrt{3}k_B T}{b\chi}\frac{1}{\alpha\xi + \beta\xi/\sqrt{\rho\phi}}. \tag{10a}$$

Alternatively, l_2^* is the controlling length scale and is on the order of the length of a GB dislocation source or the spacing between the trapped dislocations and GBs in our deformed MC pillars. We have, therefore,

$$m = \frac{\sqrt{3}k_B T}{b\chi}\frac{1}{\zeta\left(\alpha\sqrt{\rho d} + \beta\sqrt{d}\right)}. \tag{10b}$$

Here, the total dislocation density ρ stored in the grain interior can be written as

$$\rho = \rho_0 + (1 - P_{dis})\rho_n = \rho_0 + (1 - P_{dis})\varepsilon_b/(b\lambda), \tag{11}$$

where ρ_0 is the density of preexisted dislocations and that introduced by FIB milling, roughly on the order of $\sim 10^{12}$–$10^{14}/m^2$, ρ_n is the density of dislocations (either nucleated from GBs/surface or preexisted in grain interior) and can be correlated with plastic strain ε_p (maybe equal to the strain burst size ε_b) by $\rho_n = \varepsilon_p/(b\lambda)$ (Li and Chou, 1970), where λ is the dislocation mean free path proportional to d or ϕ. Taking ε_b = 0.5% for $\sigma_{2.5}$ and ε_b = 1.5% for σ_{max}, d = 180 nm and $\lambda = d$, we find that the m value calculated from Eq. (10b) changes markedly for MC pillar at different strains, whereas the V^* almost does not change during the deformation. It is consistent with present experimental results (SC pillars behave the same way). This is suggested that the deformation mechanisms of present two types of Cu pillars do not change, *i.e.*, the MC pillars deform via the operation of GBs sources, while the SC pillars deform via the collective dislocation dynamics involving dislocations interaction and multiplication (Zhu et al., 2008).

5. Conclusions

By comparing the strain rate effects on the mechanical response of submicron-sized MC and SC Cu pillars, we investigate the roles of GBs as the dislocation motion barriers and dislocation sources/sinks played in plastic deformation. Introducing GBs into SC materials can not only significantly enhance their crystalline strength and SRS but also improve the smoothness of plastic flow in a controlled and predictable manner. The presence of GBs can strongly hinder the dislocation avalanches propagation in MC pillars and suppress the intermitted strain bursts. The notable GB effects on size- and strain rate-related strain burst behaviors are semi-quantitatively explained by the model of statistical absorption of dislocations by GBs. It is the propensity for dislocations to escape at the GBs in nanocrystals that enables the shift in the mechanisms governing plasticity from forest hardening to source activation dominated. These findings provide valuable insights into the possibility of tailoring both microstructural critical sizes and sample dimensions to elicit desired plasticity.

Acknowledgements

This work was supported by the National Natural Science Foundation of China (Grant Nos. 50971097, 51201123), the 973 Program of China (Grant No. 2010CB631003), and the 111 Project of China (B06025). GL thanks the support from Fundamental Research Funds for the Central Universities and Tengfei Scholar project. JYZ thanks China Postdoctoral Science Foundation funded project for part of financial support (2012M521765). Discussions with Prof. P.J. Ferreira (University of Texas at Austin) are greatly appreciated. Access to the nanoindentation and FIB equipments in CAMP-Nano is also acknowledged.

References

Akarapu, S., Zbib, H.M., Bahr, D.F., 2010. Analysis of heterogeneous deformation and dislocation dynamics in single crystal micropillars under compression. International Journal of Plasticity 26 (2), 239–257.

Arzt, E., 1998. Size effects in materials due to microstructural and dimensional constraints: a comparative review. Acta Materialia 46 (16), 5611–5626.

Barai, P., Weng, G.J., 2009. Mechanics of very fine-grained nanocrystalline materials with contributions from grain interior, GB zone, and grain-boundary sliding. International Journal of Plasticity 25 (12), 2410–2434.
Bei, H., Shim, S., Pharr, G.M., George, E.P., 2008. Effects of pre-strain on the compressive stress–strain response of Mo-alloy single-crystal micropillars. Acta Materialia 56 (17), 4762–4770.
Bharathula, A., Lee, S.W., Wright, W.J., Flores, K.M., 2010. Compression testing of metallic glass at small length scales: effects on deformation mode and stability. Acta Materialia 58, 5789–5796.
Bitzek, E., Brandl, C., Derlet, P.M., Van Swygenhoven, H., 2008. Dislocation cross-slip in nanocrystalline fcc metals. Physical Review Letters 100 (23), 235501.
Brinckmann, S., Kim, J.-Y., Greer, J.R., 2008. Fundamental differences in mechanical behavior between two types of crystals at the nanoscale. Physical Review Letters 100 (15), 155502.
Carlton, C.E., Ferreira, P.J., 2007. What is behind the inverse Hall–Petch effect in nanocrystalline materials? Acta Materialia 55 (11), 3749–3756.
Chen, J., Lu, L., Lu, K., 2006. Hardness and strain rate sensitivity of nanocrystalline Cu. Scripta Materialia 54 (11), 1913–1918.
Cheng, S., Spencer, J.A., Milligan, W.W., 2003. Strength and tension/compression asymmetry in nanostructured and ultrafine-grain metals. Acta Materialia 51 (15), 4505–4518.
Cheng, S., Ma, E., Wang, Y.M., Kecskes, L.J., Youssef, K.M., Koch, C.C., Trociewitz, U.P., Han, K., 2005. Tensile properties of in situ consolidated nanocrystalline Cu. Acta Materialia 53, 1521–1533.
Christian, J.W., Mahajan, S., 1995. Deformation twinning. Progress in Materials Science 39 (1–2), 1–157.
Conrad, H., 2003. Grain size dependence of the plastic deformation kinetics in Cu. Materials Science and Engineering: A 341 (1–2), 216–228.
Csikor, F.F., Motz, C., Weygand, D., Zaiser, M., Zapperi, S., 2007. Dislocation avalanches, strain bursts, and the problem of plastic forming at the micrometer scale. Science 318 (5848), 251–254.
Dao, M., Lu, L., Shen, Y.F., Suresh, S., 2006. Strength, strain-rate sensitivity and ductility of copper with nanoscale twins. Acta Materialia 54 (20), 5421–5432.
Dao, M., Lu, L., Asaro, R.J., De Hosson, J.T.M., Ma, E., 2007. Toward a quantitative understanding of mechanical behavior of nanocrystalline metals. Acta Materialia 55, 4041–4065.
Dehm, G., Weiss, D., Arzt, E., 2001. In situ transmission electron microscopy study of thermal-stress-induced dislocations in a thin Cu film constrained by a Si substrate. Materials Science and Engineering: A 309–310, 468–472.
Dehm, G., Balk, T.J., Edongué, H., Arzt, E., 2003. Small-scale plasticity in thin Cu and Al films. Microelectronic Engineering 70 (2–4), 412–424.
Dehm, G., 2009. Miniaturized single-crystalline fcc metals deformed in tension: new insights in size-dependent plasticity. Progress in Materials Science 54 (6), 664–688.
Dimiduk, D.M., Uchic, M.D., Parthasarathy, T.A., 2005. Size-affected single-slip behavior of pure nickel microcrystals. Acta Materialia 53, 4065–4077.
Dimiduk, D.M., Woodward, C., Lesar, R., Uchic, M.D., 2006. Scale-free intermittent flow in crystal plasticity. Science 312 (5777), 1188–1190.
El-Awady, J.A., Rao, S.I., Woodward, C., Dimiduk, D.M., Uchic, M.D., 2011. Trapping and escape of dislocations in micro-crystals with external and internal barriers. International Journal of Plasticity 27 (3), 372–387.
El-Awady, J.A., Uchic, M.D., Shade, P.A., Kim, S.-L., Rao, S.I., Dimiduk, D.M., Woodward, C., 2013. Pre-straining effects on the power-law scaling of size-dependent strengthening in Ni single crystals. Scripta Materialia 68 (3–4), 207–210.
Farrokh, B., Khan, A.S., 2009. Grain size, strain rate, and temperature dependence of flow stress in ultra-fine grained and nanocrystalline Cu and Al: synthesis, experiment, and constitutive modeling. International Journal of Plasticity 25 (5), 715–732.
Frick, C.P., Clark, B.G., Orso, S., Schneider, A.S., Arzt, E., 2008. Size effect on strength and strain hardening of small-scale [1 1 1] nickel compression pillars. Materials Science and Engineering: A 489 (1–2), 319–329.
Friedman, N., Jennings, A.T., Tsekenis, G., Kim, J.-Y., Tao, M., Uhl, J.T., Greer, J.R., Dahmen, K.A., 2012. Statistics of dislocation slip avalanches in nanosized single crystals show tuned critical behavior predicted by a simple mean field model. Physical Review Letters 109 (9), 095507.
Greer, J.R., Oliver, W.C., Nix, W.D., 2005. Size dependence of mechanical properties of gold at the micron scale in the absence of strain gradients. Acta Materialia 53 (6), 1821–1830.
Greer, J.R., Nix, W.D., 2006. Nanoscale gold pillars strengthened through dislocation starvation. Physical Review B 73 (24), 245410-6.
Greer, J.R., De Hosson, J.T.M., 2011. Plasticity in small-sized metallic systems: intrinsic versus extrinsic size effect. Progress in Materials Science 56 (6), 654–724.
Gruber, P.A., Böhm, J., Onuseit, F., Wanner, A., Spolenak, R., Arzt, E., 2008. Size effects on yield strength and strain hardening for ultra-thin Cu films with and without passivation: a study by synchrotron and bulge test techniques. Acta Materialia 56 (10), 2318–2335.
Gu, P., Dao, M., Asaro, R.J., Suresh, S., 2011. A unified mechanistic model for size-dependent deformation in nanocrystalline and nanotwinned metals. Acta Materialia 59 (18), 6861–6868.
Hemker, K.J., Sharpe, J.W.N., 2007. Microscale characterization of mechanical properties. Annual Review of Materials Research 37, 93–126.
Huang, L., Li, Q.J., Shan, Z.W., Li, J., Sun, J., Ma, E., 2011. A new regime for mechanical annealing and strong sample-size strengthening in body-centred cubic molybdenum. Nature Communications 2, 547.
Huang, P., Wang, F., Xu, M., Xu, K.W., Lu, T.J., 2010. Dependence of strain rate sensitivity upon deformed microstructures in nanocrystalline Cu. Acta Materialia 58 (15), 5196–5205.
Inkson, B.J., Dehm, G., Wagner, T., 2002. In situ TEM observation of dislocation motion in thermally strained Al nanowires. Acta Materialia 50 (20), 5033–5047.
Jang, D.C., Cai, C., Greer, J.R., 2011. Influence of homogeneous interfaces on the strength of 500 nm diameter Cu nanopillars. Nano Letters 11, 1743–1746.
Jennings, A.T., Burek, M.J., Greer, J.R., 2010. Microstructure versus size: mechanical properties of electroplated single crystalline Cu nanopillars. Physical Review Letters 104 (13), 135503.
Jennings, A.T., Li, J., Greer, J.R., 2011. Emergence of strain-rate sensitivity in Cu nanopillars: transition from dislocation multiplication to dislocation nucleation. Acta Materialia 59 (14), 5627–5637.
Jennings, A.T., Gross, C., Greer, F., Aitken, Z.H., Lee, S.-W., Weinberger, C.R., Greer, J.R., 2012. Higher compressive strengths and the Bauschinger effect in conformally passivated copper nanopillars. Acta Materialia 60 (8), 3444–3455.
Jiang, Q., Zhang, S.H., Li, J.C., 2004. Grain size-dependent diffusion activation energy in nanomaterials. Solid State Communications 130 (9), 581–584.
Kiener, D., Grosinger, W., Dehm, G., Pippan, R., 2008. A further step towards an understanding of size-dependent crystal plasticity: in situ tension experiments of miniaturized single-crystal copper samples. Acta Materialia 56 (3), 580–592.
Kiener, D., Grosinger, W., Dehm, G., 2009a. On the importance of sample compliance in uniaxial microtesting. Scripta Materialia 60 (3), 148–151.
Kiener, D., Motz, C., Dehm, G., 2009b. Micro-compression testing: a critical discussion of experimental constraints. Materials Science and Engineering: A 505 (1–2), 79–87.
Kiener, D., Guruprasad, P.J., Keralavarma, S.M., Dehm, G., Benzerga, A.A., 2011. Work hardening in micropillar compression: in situ experiments and modeling. Acta Materialia 59 (10), 3825–3840.
Kiener, D., Minor, A.M., 2011a. Source truncation and exhaustion: insights from quantitative in situ TEM tensile testing. Nano Letters 11, 3816–3820.
Kiener, D., Minor, A.M., 2011b. Source-controlled yield and hardening of Cu(1 0 0) studied by in situ transmission electron microscopy. Acta Materialia 59 (4), 1328–1337.
Kim, J.-Y., Jang, D., Greer, J.R., 2010. Tensile and compressive behavior of tungsten, molybdenum, tantalum and niobium at the nanoscale. Acta Materialia 58, 2355–2363.
Kim, J.Y., Greer, J.R., 2009. Tensile and compressive behavior of gold and molybdenum single crystals at the nano-scale. Acta Materialia 57 (17), 5245–5253.
Kraft, O., Gruber, P.A., Mönig, R., Weygand, D., 2010. Plasticity in confined dimensions. Annual Review of Materials Research 40, 293–317.
Kunz, A., Pathak, S., Greer, J.R., 2011. Size effects in Al nanopillars: single crystalline versus bicrystalline. Acta Materialia 59, 4416–4424.

LeGoues, F.K., 1994. Self-aligned sources for dislocation nucleation: the key to low threading dislocation densities in compositionally graded thin films grown at low temperature. Physical Review Letters 72 (6), 876–879.
Li, J., Weng, G.J., 2007. A secant-viscosity composite model for the strain-rate sensitivity of nanocrystalline materials. International Journal of Plasticity 23 (12), 2115–2133.
Li, J.C.M., Chou, Y.T., 1970. The role of dislocations in the flow stress grain size relationships. Metallurgical and Materials Transactions B 1 (5), 1145–1159.
Lu, K., Lu, L., Suresh, S., 2009a. Strengthening materials by engineering coherent internal boundaries at the nanoscale. Science 324 (17), 349–352.
Lu, L., Schwaiger, R., Shan, Z.W., Dao, M., Lu, K., Suresh, S., 2005. Nano-sized twins induce high rate sensitivity of flow stress in pure copper. Acta Materialia 53 (7), 2169–2179.
Lu, L., Chen, X., Huang, X., Lu, K., 2009b. Revealing the maximum strength in nanotwinned copper. Science 323, 607–610.
Lu, L., Zhu, T., Shen, Y., Dao, M., Lu, K., Suresh, S., 2009c. Stress relaxation and the structure size-dependence of plastic deformation in nanotwinned copper. Acta Materialia 57 (17), 5165–5173.
Maaß, R., Van Petegem, S., Ma, D., Zimmermann, J., Grolimund, D., Roters, F., Van Swygenhoven, H., Raabe, D., 2009. Smaller is stronger: the effect of strain hardening. Acta Materialia 57 (20), 5996–6005.
Maaß, R., Uchic, M.D., 2012. In-situ characterization of the dislocation-structure evolution in Ni micro-pillars. Acta Materialia 60 (3), 1027–1037.
Meyers, M.A., Mishra, A., Benson, D.J., 2006. Mechanical properties of nanocrystalline materials. Progress in Materials Science 51 (4), 427–556.
Mompiou, F., Caillard, D., Legros, M., Mughrabi, H., 2012. In situ TEM observations of reverse dislocation motion upon unloading in tensile-deformed UFG aluminium. Acta Materialia 60, 3402–3414.
Mughrabi, H., 1983. Dislocation wall and cell structures and long-range internal stresses in deformed metal crystals. Acta Metallurgica 31 (9), 1367–1379.
Ng, K.S., Ngan, A.H.W., 2009. Effects of trapping dislocations within small crystals on their deformation behavior. Acta Materialia 57 (16), 4902–4910.
Norfleet, D.M., Dimiduk, D.M., Polasik, S.J., Uchic, M.D., Mills, M.J., 2008. Dislocation structures and their relationship to strength in deformed nickel microcrystals. Acta Materialia 56 (13), 2988–3001.
Oh, S.H., Legros, M., Kiener, D., Dehm, G., 2009. In situ observation of dislocation nucleation and escape in a submicron Al single-crystal. Nature Materials 8, 95–100.
Pande, C.S., Cooper, K.P., 2009. Nanomechanics of Hall–Petch relationship in nanocrystalline materials. Progress in Materials Science 54 (6), 689–706.
Raabe, D., Ma, D., Roters, F., 2007. Effects of initial orientation, sample geometry and friction on anisotropy and crystallographic orientation changes in single crystal microcompression deformation: a crystal plasticity finite element study. Acta Materialia 55 (13), 4567–4583.
Rajagopalan, J., Rentenberger, C., Peter Karnthaler, H., Dehm, G., Saif, M.T.A., 2010. In situ TEM study of microplasticity and Bauschinger effect in nanocrystalline metals. Acta Materialia 58 (14), 4772–4782.
Rao, S.I., Dimiduk, D.M., Parthasarathy, T.A., Uchic, M.D., Tang, M., Woodward, C., 2008. Athermal mechanisms of size-dependent crystal flow gleaned from three-dimensional discrete dislocation simulations. Acta Materialia 56 (13), 3245–3259.
Rinaldi, A., Peralta, P., Friesen, C., Sieradzki, K., 2008. Sample-size effects in the yield behavior of nanocrystalline nickel. Acta Materialia 56 (3), 511–517.
Schiotz, J., Jacobsen, K.W., 2003. A maximum in the strength of nanocrystalline copper. Science 301, 1357–1359.
Schneider, A.S., Clark, B.G., Frick, C.P., Gruber, P.A., Arzt, E., 2009a. Effect of orientation and loading rate on compression behavior of small-scale Mo pillars. Materials Science and Engineering: A 508 (1–2), 241–246.
Schneider, A.S., Kaufmann, D., Clark, B.G., Frick, C.P., Gruber, P.A., Monig, R., Kraft, O., Arzt, E., 2009b. Correlation between critical temperature and strength of small-scale bcc pillars. Physical Review Letters 103 (10), 105501.
Schneider, A.S., Frick, C.P., Clark, B.G., Gruber, P.A., Arzt, E., 2011. Influence of orientation on the size effect in bcc pillars with different critical temperatures. Materials Science and Engineering: A 528 (3), 1540–1547.
Schneider, A.S., Kiener, D., Yakacki, C.M., Maier, H.J., Gruber, P.A., Tamura, N., Kunz, M., Minor, A.M., Frick, C.P., 2013. Influence of bulk pre-straining on the size effect in nickel compression pillars. Materials Science and Engineering: A 559 (1), 147–158.
Schwaiger, R., Moser, B., Dao, M., Chollacoop, N., Suresh, S., 2003. Some critical experiments on the strain-rate sensitivity of nanocrystalline nickel. Acta Materialia 51 (17), 5159–5172.
Senger, J., Weygand, D., Motz, C., Gumbsch, P., Kraft, O., 2011. Aspect ratio and stochastic effects in the plasticity of uniformly loaded micrometer-sized specimens. Acta Materialia 59 (8), 2937–2947.
Shan, Z.W., Stach, E.A., Wiezorek, J.M.K., Knapp, J.A., Follstaedt, D.M., Mao, S.X., 2004. Grain boundary-mediated plasticity in nanocrystalline nickel. Science 305, 654–657.
Shan, Z.W., Mishra, R.K., Asif, S.A.S., Warren, O.L., Minor, A.M., 2008. Mechanical annealing and source-limited deformation in submicrometre-diameter Ni crystals. Nature Materials 7, 115–119.
Sneddon, I.N., 1965. The relation between load and penetration in the axisymmetric boussinesq problem for a punch of arbitrary profile. International Journal of Engineering Science 3 (1), 47–57.
Spearot, D.E., Jacob, K.I., McDowell, D.L., 2007. Dislocation nucleation from bicrystal interfaces with dissociated structure. International Journal of Plasticity 23, 143–160.
Uchic, M.D., Dimiduk, D.M., Florando, J.N., Nix, W.D., 2004. Sample dimensions influence strength and crystal plasticity. Science 305, 986–989.
Uchic, M.D., Shade, P.A., Dimiduk, D.M., 2009. Plasticity of micrometer-scale single crystals in compression. Annual Review of Materials Research 39, 361–386.
Van Swygenhoven, H., Derlet, P., Froseth, A., 2006. Nucleation and propagation of dislocations in nanocrystalline fcc metals. Acta Materialia 54, 1975–1983.
Wang, Y.M., Hamza, A.V., Ma, E., 2006. Temperature-dependent strain rate sensitivity and activation volume of nanocrystalline Ni. Acta Materialia 54 (10), 2715–2726.
Wang, Z.J., Li, Q.J., Shan, Z.W., Li, J., Sun, J., Ma, E., 2012. Sample size effects on the large strain bursts in submicron aluminum pillars. Applied Physics Letters 100, 071906.
Wei, Q., Cheng, S., Ramesh, K.T., Ma, E., 2004. Effect of nanocrystalline and ultrafine grain sizes on the strain rate sensitivity and activation volume: fcc versus bcc metals. Materials Science and Engineering A 381 (1–2), 71–79.
Wei, Q., 2007. Strain rate effects in the ultrafine grain and nanocrystalline regimes—influence on some constitutive responses. Journal of Mateials Science 42, 1709–1727.
Xie, K.Y., Shrestha, S., Cao, Y., Felfer, P.J., Wang, Y., Liao, X., Cairney, J.M., Ringer, S.P., 2013. The effect of pre-existing defects on the strength and deformation behavior of α-Fe nanopillars. Acta Materialia 61 (2), 439–452.
Yamakov, V., Wolf, D., Phillpot, S.R., Mukherjee, A.K., Gleiter, H., 2004. Deformation-mechanism map for nanocrystalline metals by molecular-dynamics simulation. Nature Materials 3 (1), 43–47.
Zhang, J.-Y., Liu, G., Wang, R.H., Li, J., Sun, J., Ma, E., 2010. Double-inverse grain size dependence of deformation twinning in nanocrystalline Cu. Physical Review B 81 (17), 172104.
Zhang, J.Y., Lei, S., Niu, J., Liu, Y., Liu, G., Zhang, X., Sun, J., 2012a. Intrinsic and extrinsic size effects on deformation in nanolayered Cu/Zr micropillars: from bulk-like to small-volume materials behavior. Acta Materialia 60 (10), 4054–4064.
Zhang, J.Y., Lei, S.Y., Liu, Y., Niu, J.J., Chen, Y., Liu, G., Zhang, X., Sun, J., 2012b. Length scale dependent deformation behavior of nanolayered Cu/Zr micropillars. Acta Materialia 60 (4), 1610–1622.
Zhang, J.Y., Liu, G., Lei, S.Y., Niu, J.J., Sun, J., 2012c. Transition from homogeneous-like to shear-band deformation in nanolayered crystalline Cu/amorphous Cu–Zr micropillars: intrinsic versus extrinsic size effect. Acta Materialia 60 (20), 7183–7196.
Zhang, J.Y., Zhang, P., Wang, R.H., Liu, G., Zhang, G.J., Sun, J., 2012d. Grain-size-dependent zero-strain mechanism for twinning in copper. Physical Review B 86 (6), 064110.

Zhang, J.Y., Cui, J.C., Liu, G., Sun, J., 2013. Deformation crossover in nanocrystalline Zr micropillars: the strongest external size. Scripta Materialia 68 (8), 639–642.
Zhou, C., Beyerlein, I.J., LeSar, R., 2011. Plastic deformation mechanisms of fcc single crystals at small scales. Acta Materialia 59 (20), 7673–7682.
Zhou, C., Biner, S., LeSar, R., 2012. Simulations of the effect of surface coatings on plasticity at small scales. Scripta Materailia 63, 1096–1099.
Zhu, T., Li, J., Samanta, A., Leach, A., Gall, K., 2008. Temperature and strain-rate dependence of surface dislocation nucleation. Physical Review Letters 100 (2), 025502.
Zhu, T., Li, J., 2010. Ultra-strength materials. Progress in Materials Science 55 (7), 710–757.